

# Heterostructure Effects on the Magnetocrystalline Anisotropy Energy of MnN.

Robert A. Lawrence<sup>1</sup>, Matt I. J. Probert<sup>1</sup>

1. School of Physics, Engineering and Technology, University of York, Heslington, North Yorkshire, YO10 5DD, UK  
March 28, 2025

## Abstract

Thin film effects on the Magnetocrystalline Anisotropy Energy (MAE) of MnN were studied using density functional theory (DFT). Initially, strain effects on bulk MnN were considered as a proxy for lattice-matching induced strain and a linear relationship between the  $c/a$  ratio and the MAE was found. This relationship was explained in terms of underlying point group symmetry. Strain and charge-transfer effects were then considered for an ultra-thin film. It was found that a Ta seed-layer suppresses the net spin moment on the Mn ions, leading to a reduction of the MAE.

## 1 Introduction

At the heart of many spintronic devices is an interface between a magnetically anisotropic layer and another magnetic system [1]. Optimising these devices, including through material discovery, is currently a significant driver of research activity.

In addition to experimental searches, computational research into magnetic materials provides significant insight into underlying materials properties. In addition to providing a financially cheaper route to screen materials, computational techniques also enable counterfactual or experimentally unrealisable configurations to be considered. This in turn enables effects to be separated and the creation of general principles to guide future searches for high-performance materials.

To date, most of the *ab initio* computational effort in magnetocrystalline anisotropy has been concerned with bulk systems of infinite crystals [2, 3, 4]. While important for finding novel high performance magnetic materials, the results of these simulations tend to agree relatively poorly with experimental equivalents. One possible reason for this is the difference between an infinite bulk crystal and a thin layer of material within a heterostructure.

In this paper, we will investigate the effects of common interfacial physics on the magnetocrystalline anisotropy energy (MAE) of MnN, an important material due to its having a high MAE for a system that does not contain scarce elements such as Ir and Pt.

### 1.1 Background Theory

There are many physical processes that happen when two materials are brought together to form an interface. It will be the aim of this paper to – as far as is possible – separate out these variables for independent investigation. For certain variables, this is not achievable, even within a density functional model.

### 1.2 Shape Anisotropy

When comparing infinite bulk MnN with a bilayer system, one must also consider the effects of shape anisotropy. This will be controlled by performing MAE calculation involving the same bilayer structure, enabling the difference due to the applied effects to be highlighted without attributing these changes to shape anisotropy. Shape anisotropy must however, be considered when making comparisons between the bulk and thin film limits.

### 1.3 Fermi Level Equilibration and Charge Transfer

An additional of interfaces is the redistribution of electrons from one side of the interface to another. This process is driven by Fermi level equilibration [5]. This can lead to a net accumulation of charge on one side of the interface, and a depletion of charge on the other. Along with the change in the local charge, one would also expect a change to the local *spin*. This is somewhat harder to predict however, as adding an electron to a high spin complex with

greater than or equal to half occupancy of the d- (or f-) subshell will decrease the net spin moment, whereas for a system with less than half occupancy it will increase it. A further complication to this is that we are dealing with a quantum mechanical system, and therefore expectation values which means that partial occupancies are valid.

A useful proxy value for this is electronegativity, which is defined as “the ability of an atom to attract an electron towards itself within a covalent bond”. For an interface, one may use this alongside *ceteris paribus* thinking to make a rough conclusion about what will happen to the number of electrons at a site; ignoring itinerant (delocalised) magnetism, this is sufficient to determine what will happen to the local spin moments. MAE is strongly correlated with net moment as it takes less energy to rotate a smaller spin moment than a larger one.

Within DFT simulations, this effect may be quantified by comparing site projections of the spin and charge density, using schemes such as Mulliken decomposition [6].

## 1.4 Lattice Matching and Strain

One of the simplest effects to describe (and easiest to isolate) is the effects of lattice matching. A lattice mismatch prohibits bonding due to the lack of overlap of atomic orbitals (assuming we work within an LCAO type approximation for bonding!) To counter this, the two materials on either side of the interface deform such that they tend towards the average lattice parameters of the two materials. This induces a strain in both, which is energetically unfavourable compared with the infinite bulk state, but enables more atomic overlap, so greater bonding-related stabilisation resulting in a net reduction of the interfacial energy. An additional factor when growing crystals is that some *relative orientations* of the two crystals have less lattice mismatch than others, leading to different miller planes being orthogonal to the growth direction depending on the precise choice of substrate/seed layers in the stack.

In the high-strain limit, it is generally preferable to introduce defects rather than to strain the material too severely, which induces extra complications. As with compositional changes due to diffusion, we neglect these defects in this paper due to their high cost of simulation and general undesirability meaning they are not typically selected for in material growth.

Within DFT simulations, the strain effects may be added simply by straining the isolated cell in the same way (i.e. uniaxial vs biaxial vs hydrostatic) as is found in the real system. Many previous studies [4, 7] have shown strain to be a powerful control for magnetocrystalline anisotropy, with both the magnitude and sign of any uniaxial anisotropy being strain dependent.

A classic example of this is bulk Fe, which with its body centred cubic (bcc) structure has octahedral point groups ( $O_h$  in Schönflies notation) at each of its atomic centres. This has degenerate  $d_{xy}$ ,  $d_{xz}$  and  $d_{yz}$  orbitals in a so-called  $t_{2g}$  set, and a further  $e_g$  set consisting of the  $d_{z^2}$  and  $d_{x^2-y^2}$  orbitals. This symmetry in turn gives rise to the cubic anisotropy that is well recorded for bulk Fe (The small deviations from uniform charge yields the small . If Fe is strained uniaxially or biaxially, then certain symmetry operations are broken, reducing the point group to  $D_{4h}$ . This has a unique fourfold ( $C_4$ ) rotation axis, which implies a uniaxial anisotropy. The nature of this axis, magnetically hard or easy, depends on the sign of the strain and is not determined by the point group. In this sense, the qualitative changes to anisotropy induced by strain may be understood through a crystal field theory like approach, even if the quantitative changes still require a more sophisticated electronic theory technique to predict.

These effects may be investigated through applying a direct strain to the isolated layer. Appropriate degrees of strain for the simulation may be considered by

## 1.5 Disorder

Throughout this work, we will consider atomically sharp interfaces. In practice, growing such interfaces is an enormous technical challenge, with ionic diffusion and various point defects having a significant role [8]. Disorder such as this has many effects on the system, varying from breaking of local symmetry to charge and spin redistribution. Whilst these effects are significant, and should not be neglected, we elect to focus this work on atomically sharp interfaces to reduce the complexity of the problem and enable concentration on the interfacial effects alone.

## 2 Computational Methods

Density functional theory (DFT) simulations were performed using CASTEP [9], a plane-wave pseudopotential based DFT code. A plane-wave cut-off energy of 1800 eV was used in conjunction with a Monkhorst-Pack grid[10] of  $20 \times 20 \times 20$  for the Bulk MnN and a  $20 \times 20 \times 1$  grid for the ultra-thin MnN films, with the single k-point representing the aperiodic direction. Total energies were converged to  $1 \times 10^{-10}$  eV/Å. Structures were

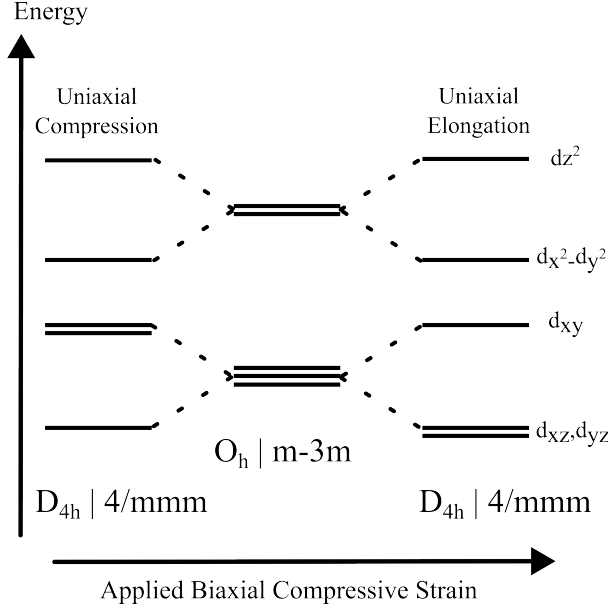


Figure 1: Schematic of changing crystal field splitting against relative uniaxial elongation / compression of an octahedral point group. The magnitude of the splitting depends on the magnitude of the charges that cause the splitting.

relaxed with a two-point steepest descent algorithm until forces were better than  $1 \times 10^{-2} eV/\text{\AA}$  and the total energy difference between configurations was better than  $1 \times 10^{-2} eV/\text{atom}$ .

To construct the unit cells of ultra-thin film MnN, an initial seed layer of [111] Ta was created and relaxed. A thin layer of MnN was then placed on top under two different translations (with the Mn or the N lying directly on top of the Ta) and relaxed. In both cases H-passivation was used to minimise the amount of vacuum gap required to minimise spurious self-interaction of the polar surface with its periodic images. The configuration with N on top of the Ta (see panel a of figure 2) was found to be the lowest energy and used thereafter. Finally, to generate extra configurations the Ta and H-passivation layers were removed with no further changes to the unit cell. These are therefore not experimentally realisable systems, but enable direct comparison with the ultra-thin film on Ta (configuration a).

Requiring the structure not to change also enforced rotating the spin moment without allowing the atoms to relax. For the MAE of the bulk system; the relaxation method outlined in [11] was used. Relaxation of the ionic degrees of freedom while at the magnetically hard electronic configuration reduced the MAE by  $9\mu eV/\text{ion}$ .

## 2.1 Surface Reconstruction

In contrast to the infinite bulk case, the edge of the MnN relaxes into the vacuum gap. This is an expected form of surface reconstruction, and is not inhibited by the hydrogen passivation. We note that this is an effect caused by our ultra-thin layer of MnN, and would also not be expected for a capped system. Nevertheless, the results we find on the change of MAE do not depend on the surface reconstruction: the reconstruction is present every ultra-thin film system, so when conclusions about underlying mechanisms are considered by studying different configurations, the surface relaxation is kept constant.

## 3 Results and Discussion

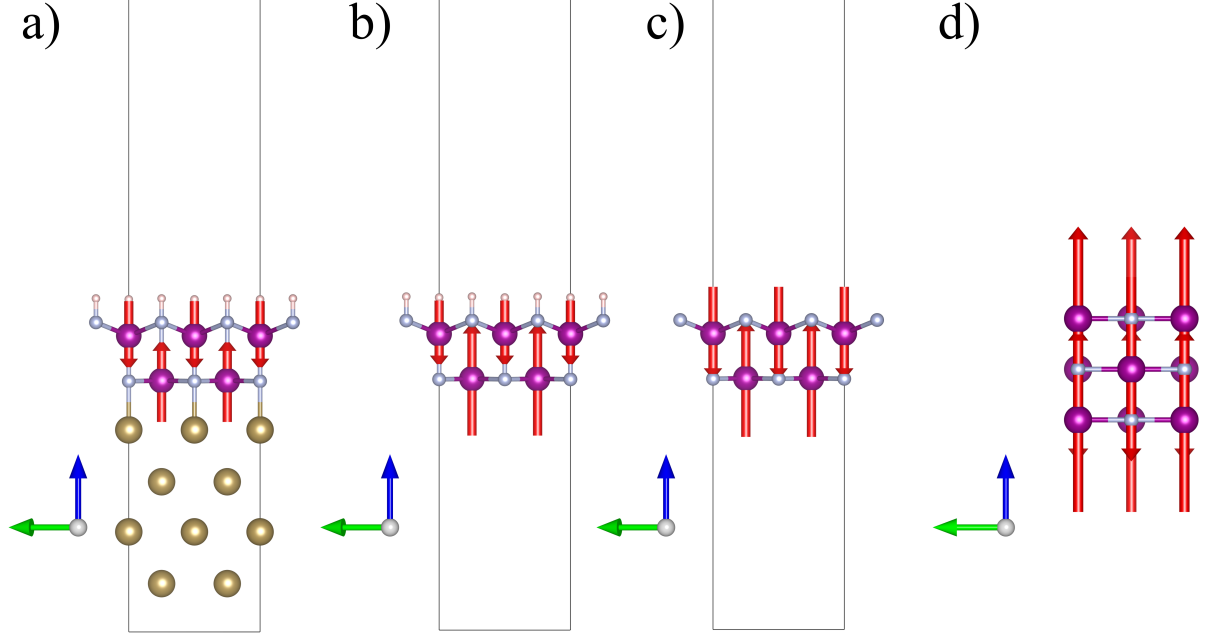


Figure 2: a) H (light pink) -passivated Mn (purple) N (light blue) bilayer on Ta (bronze), b)

H-passivated MnN bilayer, c) MnN bilayer, d) Bulk MnN. Spins are represented by red arrows, with the length of the arrow representing the per-site projection of the spin density. Spin Magnitudes are reported in table 1

### 3.1 Strain effects on Bulk MnN

One of the most important effects to be considered when growing a thin film is lattice matching. To investigate this further, we begin by considering the effects of strain on the MAE of bulk  $\theta$ -phase MnN, before considering the thin-film limit.

For each case, a biaxial strain was applied to the  $\vec{a}, \vec{b}$  lattice vectors, and the MAE calculated both with and without the relaxation of the  $\vec{c}$  lattice vector. For the unrelaxed cases, an arbitrary value of  $\vec{c} \approx 4\text{\AA}$ , was chosen. The MAE was then plotted against the effective  $\frac{|\vec{c}|}{|\vec{a}|}$  ratio of the system (see figure 3) and both linear and quadratic regressions were performed. The line of best fit for the data is given by

$$\text{MAE} = -5.1005 + 5.33375 \cdot \frac{|\vec{c}|}{|\vec{a}|} \text{ meV/formula unit} \quad (1)$$

which has a \*regression data here\*.

however it should be noted that this is only interpolative for small levels of strain.

Firstly, we note that the point group of the ions in MnN is, in Schönflies notation,  $D_{4h}$ , which is a subset of the octahedral ( $O_h$ ) point group, which is the special case for cubic symmetry. Elongation ( $c/a > 1$ ) and compression ( $c/a < 1$ ). For this subset of symmetries, which also applies to well-known magnetic materials such as FeCo, FePt and PtMn that also show this linear trend [4, 11].

Now, it is instructive to consider a multipole expansion of the so-called crystal field (the electrostatic potential due to the uneven distribution of charge in the system) about the Mn ions. As we change the  $c/a$  ratio, we find that we both change the quadrupole moments (which are the only moments that can interact with d-orbitals due to the symmetry of the perturbation from spherical) and the monopole moment (which provides a rigid shift to the energy that cancels when evaluating MAE). This may be seen in figure 1, which also notes that for the special case of  $c/a=1$  we have octahedral crystal field splitting.

For an isolated atom, the octahedral splitting would cause cubic anisotropy, such as is observed with bulk Fe, however for binary systems such as MnN, FePt and PtMn, this is not the case. This is due to the fact that in a heteronuclear system the charge imbalances are much higher; the magnitude of the crystal field splitting is much smaller for BCC Fe than in the example binary systems.

In these systems the “magnetic” ion (Fe or Mn) also experiences a change in spin moment between alignment along the  $\vec{a}$  and  $\vec{c}$  direction. Pairing electrons within the same spatial orbital, which is required in order

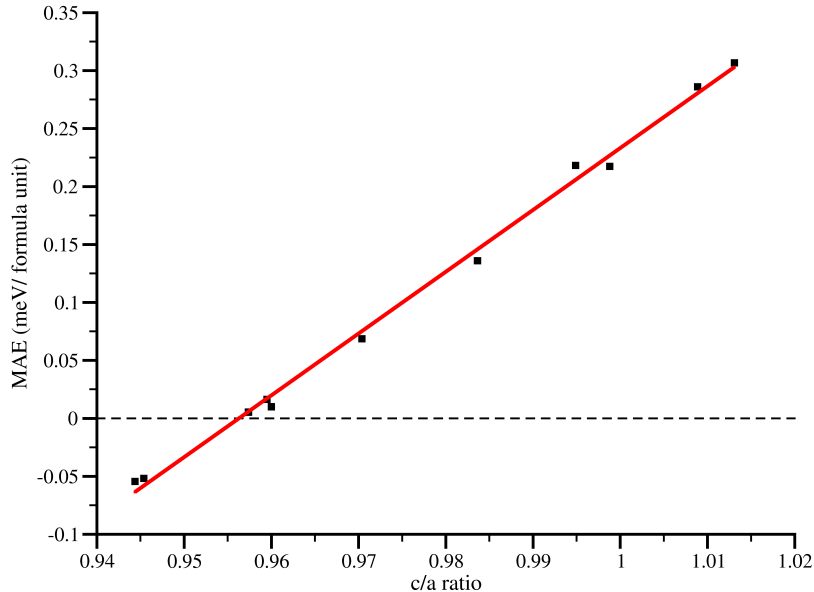


Figure 3: MAE (in meV/ formula unit) against the  $c/a$  ratio for bulk phases of MnN. Both the unit cells with relaxed  $\vec{c}$  and unrelaxed  $\vec{c}$  lie on the same line.

to change the orientation of the net spin has an associated energy penalty, due to the increased Coulombic repulsion due to the reduced average separation between electrons in the same spatial orbital (the opposite spins ensure agreement with the Pauli principle).

Next, we note this argument neglects the effects of bonding interactions; this is based upon the use of the expansion postulate and noting that the spherical harmonics for  $\uparrow=2$  are a complete basis for describing localised d-orbitals. Accordingly, the bonding interactions are accounted for by their effect on the effective occupations of the basis functions for a given spin configuration.

Now, under these approximations we may express the MAE of the system as

$$MAE = \sum_i \Delta f_i \cdot \epsilon_i(c/a) + \Delta E_{spin-pairing} \quad (2)$$

where  $\Delta f_i$  is the change in effective occupancies of the spherical harmonic basis between the minimum energy electronic configuration that leads to a net spin aligned along  $\vec{z}$  and the minimum energy of the electronic configuration that leads to a net spin aligned along  $\vec{x}$  (here we use  $x$  to represent the direction associated with the hard axis of the relaxed bulk phase).  $\Delta E_{spin-pairing}$  is the additional Coulombic energy penalty associated with the enhanced repulsive correlation due to two electrons occupying the same spatial orbital. This spin-pairing energy depends on the basis functions, so does not change with  $c/a$ , and for a sufficiently small change in the bonding the  $\frac{1}{|\vec{r}|}$  potential from each charge also means the quadrupole term in the multipole expansion changes linearly with  $c/a$  ratio.

### 3.1.1 Applicability to Other Magnetic Systems

The linear relationship of strain to MAE has previously been reported for other systems, such as FePt and PtMn [11], as well as bulk Fe. These systems all have in common that biaxial strain causes them to pass from a  $D_{4h}^+$  to a  $D_{4h}^-$  system, while passing through an  $O_h$  configuration (we note that for bulk Fe, the  $O_h$  configuration is the ground state BCC structure). This explanation in terms of the underlying point group symmetry for the magnetic ion also explains the underlying trend in these systems. This enables us to state that this will be a common trend in all materials where the point group of the “magnetic” ions are all  $D_{4h}$  with a common rotation axis. Finally, we note that this also applies to the  $O_h$  point group, which is a super-set of the  $D_{4h}$  point group. The authors also conject that a similar mechanism may also affect the entire  $D_{nh}$  class, making this applicable to most uniaxial magnetic systems.

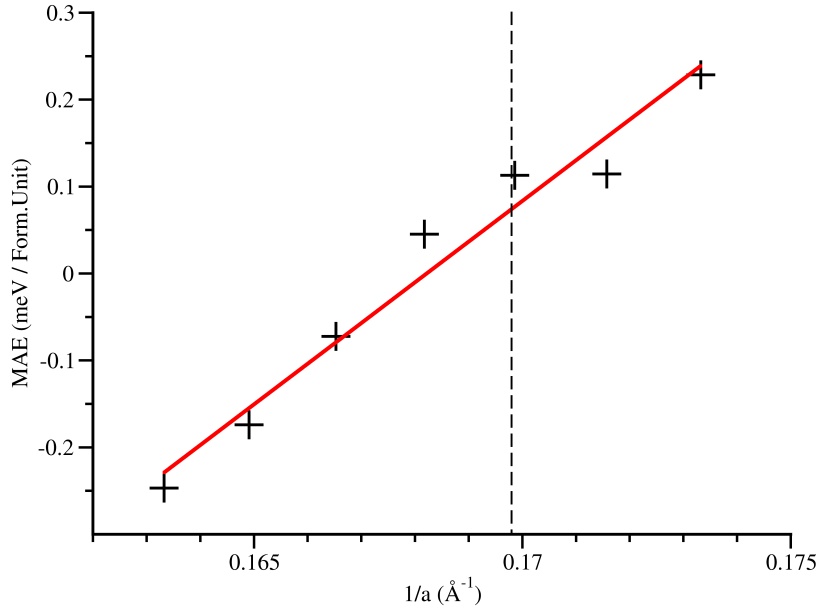


Figure 4: MAE for the ultrathin film case of MnN shown in panel b of figure 2. The vertical black dotted line indicates the inverse lattice parameter for MnN on a Ta seed layer.

### 3.2 Strain Effects in the Ultra-thin Film Limit

Strains were also applied to an ultrathin film of H-passivated MnN (see panel b, figure 2), and the value of the MAE against the inverse of the  $\bar{a}$  lattice constant was recorded. A  $c/a$  ratio was not used due as the  $\bar{c}$  lattice vector was kept fixed throughout these simulations (and is somewhat ill-defined for a thin-film in vacuum). The results of these are shown in figure 4, with a line of best fit given by

$$MAE = \frac{46.805}{|\bar{a}|} - 7.8735 \text{ meV / form.unit} \quad (3)$$

for MAE in meV/formula unit and  $\bar{a}$  measured in Angstroms. We emphasise that this equation is for the ultra-thin film limit, for a system that is unlikely to be experimentally realisable.

We also note that the system underwent a change in-plane, with the elongation of one of the in-plane axes in order to better lattice-match with the Ta. This reduced the symmetry from a  $D_{4h}$  to a  $D_{2h}$  system, and accordingly an intermediate as well as hard axis was seen in-plane. The intermediate axis (bisecting the bonds) was lower in energy and this is the MAE value reported for these systems, as is the value relevant to spin flipping events (which are dominated by the lowest-energy saddle point between two potential wells). This is in agreement with the earlier comments on the crystal field effects, and a linear relationship of MAE is still expected (as seen in figure 4).

### 3.3 Non-Strain Effects of a Seed Layer

Strain is not, however, the only effect to occur when changing from bulk to thin film. We will continue our investigation by considering the growth of an ultra-thin film of MnN on [111] Ta. Whilst this system is too thin to necessarily represent an experimentally realisable system, it emphasises the subtle effects that may be expected, and makes a qualitative, transferable, analysis of the relevant physical mechanisms simpler.

To this end, we start by studying an ultra-thin film of MnN grown on a layer of [111] Ta, which is a popular choice for experimental growth of MnN [12, 13], with an additional H passivation layer to suppress the net dipole moment and allow for the use of a smaller unit cell. Two interface configurations were chosen – with either the Mn or N on top of the Ta atoms, and the lower energy configuration following a geometry optimisation (N on top of Ta) was selected for further investigation. Then, the seed layer and H-passivation layers were removed with all other parameters kept the same (See figure 2).

As well as inducing an applied strain, the seed layer also interacts with the thin film chemically – there is a transfer of electrons between the two systems. This effect, which is driven by Fermi level equilibration, leads to a change of the net spin moments in the system and also affects the MAE. The Mulliken spin projections

Subfigure	Mn (lower) $/\mu_B$	Mn (upper) $/\mu_B$	MAE ( $\mu_e$ V/ion)
a)	1.77	-1.48	86
b)	2.43	-1.42	113
c)	2.50	-1.99	39
d)	3.55	-3.55	127

Table 1: Simulated spin magnitudes and magnetocrystalline anisotropy energies for the 4 structures presented in figure 2. The upper layer is reconstructed in subfigures a, b, c and H-passivated in subfigures a and b. subfigure a also features a Ta layer, leading to the suppression of the net spin moment in the lower layer. Negative spin moments indicates spin down, and positive moments indicate spin up.

on the atoms are shown in table 1. From this, it is possible to see that both the H-passivation layer and the Ta seed layer cause an electron transfer that quenches the spin in the MnN ultrathin layer.

It is worth noting that the vacuum spacing was not changed when removing the H-passivation layer for configuration c). One potential effect of this in periodic boundary conditions is to apply a dipole field across the system. This may explain the anomalously low MAE that is not present in bulk or the H-passivated thin films,

From these data, it is possible to conclude that not only lattice matching, but also the degree of charge transfer between layers is important when designing a device where magnetic anisotropy of one layer is important. The suppression of spin moments by Ta may also explain why high thicknesses of MnN [12] are required in order to make the material perform well; this suppression will decay back towards bulk values as a thicker film is constructed. We also note that a ferromagnetic capping layer, commonly used in devices in conjunction with antiferromagnets such as MnN, may also have similar effects, and that consideration of charge transfer at the ferromagnet-antiferromagnet interface will be important future work.

## 4 Conclusions

Density Functional Theory was used to study the effects of forming a simple heterostructure on magnetocrystalline anisotropy energy (MAE) for MnN and Ta. Strain effects were investigated for the bulk and ultra-thin film limits, and a linear relationship between the  $c/a$  ratio and MAE was found with both relaxed and unrelaxed simulation cells being on the same line for the bulk case. An explanation for this linear relationship in terms of crystal field theory was given and the applicability of this linear trend to all uniaxial systems was posited. Within the ultra-thin film limit, the MAE was also found to vary depending on the presence of nearby layers, which was significantly driven by charge transfer induced by Fermi level equilibration leading to spin quenching, especially in the layer immediately forming the interface.

## References

- [1] Benedetta Flebus, Dirk Grundler, Bivas Rana, YoshiChika Otani, Igor Barsukov, Anjan Barman, Gianluca Gubbiotti, Pedro Landeros, Johan Akerman, Ursula Ebels, Philipp Pirro, Vladislav E Demidov, Katrin Schultheiss, Gyorgy Csaba, Qi Wang, Florin Ciubotaru, Dmitri E Nikonov, Ping Che, Riccardo Hertel, Teruo Ono, Dmytro Afanasiev, Johan Mentink, Theo Rasing, Burkard Hillebrands, Silvia Viola Kusminskiy, Wei Zhang, Chunhui Rita Du, Aurore Finco, Toeno van der Sar, Yunqiu Kelly Luo, Yoichi Shiota, Joseph Sklenar, Tao Yu, and Jinwei Rao. The 2024 magnonics roadmap. *Journal of Physics: Condensed Matter*, 36(36):363501, June 2024.
- [2] L. Szunyogh, B. Lazarovits, L. Udvardi, J. Jackson, and U. Nowak. Giant magnetic anisotropy of the bulk antiferromagnets  $\text{irmn}$  and  $\text{irmn}_3$  from first principles. *Physical Review B*, 79(2), January 2009.
- [3] J. B. Staunton, S. Ostanin, S. S. A. Razee, B. L. Gyorffy, L. Szunyogh, B. Ginatempo, and Ezio Bruno. Temperature dependent magnetic anisotropy in metallic magnets from an ab initio electronic structure theory:  $1l_0$ -ordered fept. *Physical Review Letters*, 93(25), December 2004.
- [4] Michael Wolloch and Dieter Suess. Strain-induced control of magnetocrystalline anisotropy energy in feo thin films. *Journal of Magnetism and Magnetic Materials*, 522:167542, March 2021.
- [5] Pekka Peljo, José A. Manzanares, and Hubert H. Girault. Contact potentials, fermi level equilibration, and surface charging. *Langmuir*, 32(23):5765–5775, June 2016.

- [6] R. S. Mulliken. Electronic population analysis on lcao–mo molecular wave functions. i. *The Journal of Chemical Physics*, 23(10):1833–1840, October 1955.
- [7] Chengyang Zhao, Shiming Yan, Shiran Gao, Wen Qiao, Ru Bai, and Tiejun Zhou. Strain-control magnetic anisotropy of antiferromagnetism in two-dimensional mxene v2c(oh)2. *The Journal of Physical Chemistry C*, 128(47):20350–20359, November 2024.
- [8] K. A. Thórarinsdóttir, N. Strandqvist, V. V. Sigurjónsdóttir, E. B. Thorsteinsson, B. Hjörvarsson, and F. Magnus. Finding order in disorder: Magnetic coupling distributions and competing anisotropies in an amorphous metal alloy. *APL Materials*, 10(4), April 2022.
- [9] Stewart J. Clark, Matthew D. Segall, Chris J. Pickard, Phil J. Hasnip, Matt I. J. Probert, Keith Refson, and Mike C. Payne. First principles methods using castep. *Zeitschrift für Kristallographie - Crystalline Materials*, 220(5–6):567–570, May 2005.
- [10] Hendrik J. Monkhorst and James D. Pack. Special points for brillouin-zone integrations. *Physical Review B*, 13(12):5188–5192, June 1976.
- [11] Robert A. Lawrence, Scott J. Donaldson, and Matt I. J. Probert. Magnetic transition state searching: Beyond the static ion approximation. *Magnetochemistry*, 9(2):42, January 2023.
- [12] M. Dunz, T. Matalla-Wagner, and M. Meinert. Spin-orbit torque induced electrical switching of antiferromagnetic mnn. *Physical Review Research*, 2(1), March 2020.
- [13] Gonzalo Vallejo-Fernandez and Markus Meinert. Recent developments on mnn for spintronic applications. *Magnetochemistry*, 7(8):116, August 2021.